Acta Biomaterialia 52 (2017) 81–91

Contents lists available at ScienceDirect

Acta Biomaterialia

journal homepage: www.elsevier.com/locate/actabiomat

Full length article

Moldable elastomeric polyester-carbon nanotube scaffolds for cardiac tissue engineering ☆

Samad Ahadian [a,1], Locke Davenport Huyer [a,b,1], Mehdi Estili [c], Bess Yee [b], Nathaniel Smith [b], Zhensong Xu [d], Yu Sun [d], Milica Radisic [a,b,*]

[a] Institute of Biomaterials and Biomedical Engineering, University of Toronto, Toronto, Ontario, Canada
[b] Department of Chemical Engineering and Applied Chemistry, University of Toronto, Toronto, Ontario, Canada
[c] Ceramics Processing Group, Research Center for Functional Materials, National Institute for Materials Science (NIMS), Tsukuba, Japan
[d] Advanced Micro and Nanosystems Laboratory, Department of Mechanical and Industrial Engineering, University of Toronto, Toronto, Ontario, Canada

ARTICLE INFO

Article history:
Received 7 September 2016
Received in revised form 11 November 2016
Accepted 6 December 2016
Available online 8 December 2016

Keywords:
Carbon nanotubes
Scaffold
Cardiac tissue engineering
Elastomer
Electrical conductivity
Maturation

ABSTRACT

Polymer biomaterials are used to construct scaffolds in tissue engineering applications to assist in mechanical support, organization, and maturation of tissues. Given the flexibility, electrical conductance, and contractility of native cardiac tissues, it is desirable that polymeric scaffolds for cardiac tissue regeneration exhibit elasticity and high electrical conductivity. Herein, we developed a facile approach to introduce carbon nanotubes (CNTs) into poly(octamethylene maleate (anhydride) 1,2,4-butanetricarboxylate) (124 polymer), and developed an elastomeric scaffold for cardiac tissue engineering that provides electrical conductivity and structural integrity to 124 polymer. 124 polymer-CNT materials were developed by first dispersing CNTs in poly(ethylene glycol) dimethyl ether porogen and mixing with 124 prepolymer for molding into shapes and crosslinking under ultraviolet light. 124 polymers with 0.5% and 0.1% CNT content (wt) exhibited improved conductivity against pristine 124 polymer. With increasing the CNT content, surface moduli of hybrid polymers were increased, while their bulk moduli were decreased. Furthermore, increased swelling of hybrid 124 polymer-CNT materials was observed, suggesting their improved structural support in an aqueous environment. Finally, functional characterization of engineered cardiac tissues using the 124 polymer-CNT scaffolds demonstrated improved excitation threshold in materials with 0.5% CNT content (3.6 ± 0.8 V/cm) compared to materials with 0% (5.1 ± 0.8 V/cm) and 0.1% (5.0 ± 0.7 V/cm), suggesting greater tissue maturity. 124 polymer-CNT materials build on the advantages of 124 polymer elastomer to give a versatile biomaterial for cardiac tissue engineering applications.

Statement of Significance

Achieving a high elasticity and a high conductivity in a single cardiac tissue engineering material remains a challenge. We report the use of CNTs in making electrically conductive and mechanically strong polymeric scaffolds in cardiac tissue regeneration. CNTs were incorporated in elastomeric polymers in a facile and reproducible approach. Polymer-CNT materials were able to construct complicated scaffold structures by injecting the prepolymer into a mold and crosslinking the prepolymer under ultraviolet light. CNTs enhanced electrical conductivity and structural support of elastomeric polymers. Hybrid polymeric scaffolds containing 0.5 wt% CNTs increased the maturation of cardiac tissues fabricated on them compared to pure polymeric scaffolds. The cardiac tissues on hybrid polymer-CNT scaffolds showed earlier beating than those on pure polymer scaffolds. In the future, fabricated polymer-CNT scaffolds could also be used to fabricate other electro-active tissues, such neural and skeletal muscle tissues. In the future, fabricated polymer-CNT scaffolds could also be used to fabricate other electro-active tissues, such as neural and skeletal muscle tissues.

1. Introduction

Heart failure and diseases still remain as a major cause of death for people around the world, while there are limited modalities to treat them [1]. A recent study estimated that approximately

☆ Part of the Special Issue on Extracellular Matrix Proteins and Mimics, organized by Professor Katja Schenke-Layland.

* Corresponding author at: Institute of Biomaterials and Biomedical Engineering, University of Toronto, Toronto, Ontario M5S 3G9, Canada.
E-mail address: m.radisic@utoronto.ca (M. Radisic).

[1] These authors contributed equally to this work.

http://dx.doi.org/10.1016/j.actbio.2016.12.009
1742-7061/

38 million people have experienced a heart failure during their life and this number tends to increase with the age of the population [2]. Although prevention strategies are improving, current treatment methods involve heart maintenance with pharmaceuticals and transplants, both of which are non-sustainable. Moreover, adult cardiomyocytes (CMs) are terminally differentiated cells and have minimal intrinsic ability to self-regenerate [3]. These limitations have motivated people to develop strategies for cardiac tissue regeneration.

Tissue engineering (TE) generally aims to restore or regenerate the structure and function of native cardiac tissues. TE approaches often employ cells and natural or synthetic biomaterials as the scaffold in fabricating cardiac tissues. Cardiac progenitor cells are cultured and matured onto the scaffold to make a functional cardiac tissue *in vitro* [4]. Electrical and mechanical stimulations can further be applied to engineered tissues to improve their cellular alignment, metabolic activity, and contractility [5,6]. Structure, biodegradation, elasticity, cell affinity, and inflammatory response of scaffolds are important parameters that need to be controlled to construct a functional cardiac tissue [4]. An ideal scaffold should mimic physiological properties and function of extracellular matrix (ECM) in the native myocardium.

Different natural and synthetic polymers have been used as scaffolding materials for cardiac TE including polyurethane [7], poly(glycerol sebacate) [8], alginate [9], gelatin [10], and their blends [11,12]. In general, each scaffold targets certain properties of the ECM in the native cardiac tissue. Incorporation of bionanomaterials (*e.g.*, carbon nanotubes (CNTs) [13,14] and graphene [15,16]) have also been used in scaffolds for engineered cardiac tissues to improve their mechanical and electrical properties. For example, Shin et al. synthesized CNT-incorporated gelatin methacryloyl hydrogel and used it for cardiac TE [17], which demonstrated higher Young's modulus and electrical conductivity compared to the pristine hydrogels. In addition, neonatal rat CMs seeded onto the CNT hydrogels had higher electrophysiological activity and maturation compared to the cells cultured onto the pristine hydrogels. In another study, Martinelli et al. showed CMs tightly adhered to CNT substrates increasing their viability, proliferation, and maturation [18]. They claimed that CNTs have great potential in manipulating nanoscale dimensions of ECM. Graphene oxide has also been proposed to enhance mechanical characteristics of methacryloyl-substituted recombinant human tropoelastin [19,20]. A higher rate of beating was reported for cardiac tissues fabricated on hybrid graphene oxide-hydrogel scaffolds compared to pristine hydrogel scaffolds due to higher electrical signal propagation in the hybrid gels. Carbon-based nanomaterials have also been combined with other polymeric biomaterials, such as poly (glycerol sebacate):gelatin [21], poly(ethylene glycol)-poly(D,L-lactide) copolymer [22], and poly(lactic-co-glycolic acid) [23] to regulate the behavior and function of CMs. Superior performance of hybrid carbon-based nanomaterial-polymer scaffolds in cardiac tissue regeneration is mainly due to high electrical conductivity and mechanical strength of the nanomaterials [16,24].

In our previous work, a highly elastic polyester, poly(octamethylene maleate (anhydride) 1,2,4-butanetricarboxylate) (124 polymer), was synthesized for the first time and used as the scaffold for cardiac TE [25]. However, 124 polymer is not highly conductive, limiting its performance in regulating cardiac cell behaviors and function. Moreover, 124 polymer has significant structural change in aqueous media upon the removal of poly (ethylene glycol) dimethyl ether as the porogen from the polymer network limiting precise control of the scaffold design and architecture. In this work, we present the synthesis of hybrid 124 polymer-CNT materials. With the introduction of CNTs to 124 polymer, we hypothesized that electrical conductivity and structural support in 124 polymer-CNT materials. 124 polymer-CNT materials were characterized, and used as the scaffold in cardiac TE constructs to assess viability and function of neonatal rat CMs within them.

2. Materials and methods

2.1. Prepolymer synthesis

124 prepolymer was synthesized as previously described [25]. Briefly, 5 g 1,2,4-butanetricarboxylic acid (Sigma-Aldrich), 21.15 g 1,8-octanediol (Sigma-Aldrich), and 10.31 g maleic anhydride (Sigma-Aldrich) were mixed in a 250-mL round-bottom flask under nitrogen flow. The ratios of hydroxyl to carboxylic end groups and 1,2,4-butanetricarboxylic acid to maleic anhydride were kept at 1:1 and 1:4, respectively. The contents of the reaction vessel were melted at 150 °C with stirring at 200 rpm for 5 h. Crude prepolymer was then dissolved in 1,4-dioxane (Sigma-Aldrich) and purified with dropwise precipitation through deionized distilled water. The purified prepolymer was collected and concentrated under airflow for 48 h.

2.2. Development of 124 polymer-CNT materials

Multi-walled CNTs were purchased from Hodogaya Chemical Co., Ltd, Japan (diameters in the range of 40–90 nm and length 10–20 μm). The CNTs were functionalized as described previously with a controlled acid treatment process [14]. In short, CNTs were refluxed at 110 °C for 20 min in a 1:3 (vol) mixture of 68% (wt) nitric acid and 98% (wt) sulfuric acid, respectively. Functionalized CNTs were then washed in pure water on a 1.2 μm membrane and dispersed in water using probe sonication to prepare a highly stable aqueous dispersion and generate a stock solution. This solution was used to make 124-CNT prepolymer (Fig. 1A). First, an aliquot of stock solution was dried overnight at 80 °C to give CNT powder. The powder was combined with poly(ethylene glycol) dimethyl ether (PEGDM) as the porogen (Sigma-Aldrich) at the desired concentration (wt%), then stirred and sonicated at 50 °C for 90 min to evenly disperse the CNTs within the fluid (0, 0.5, or 1.5% CNT content). The CNT-porogen mixture was added to 124 polymer at 50% (wt/wt) concentration. The resulting polymer was mixed with UV initiator (2-hydroxyl-1-[4(hydroxyethoxy)-phenyl]-2-methyl-1 propanone, Irgacure 2959, 5% (wt), Sigma-Aldrich) at 100 °C. This solution was then exposed to UV light to give final crosslinked polymer structures.

2.3. Raman spectroscopy

Molecular vibrational frequencies of 124 polymer-CNT materials were recorded using Raman spectrometer (SENTERRA II Compact Raman Microscope, Bruker Corp., USA). A 532 nm laser beam was used with the laser power of 20 mW and the resolution of 3–5 cm^{-1}. Peak intensity was measured for each sample and represented graphically.

2.4. Electrical characterization

Polymer strips were used for current-voltage measurements. The strips were prewetted with Dulbecco's phosphate-buffered saline (DPBS) for 5 min and then the DPBS was removed prior to the measurement. Current-voltage curves of polymers were revealed by applying DC currents through a current source (Model 6221 DC and AC current source, Keithley, USA). The voltage between two endpoints of strips was recorded using a digital multimeter (Model 381275, Extech Instruments, USA). Solution's ionic

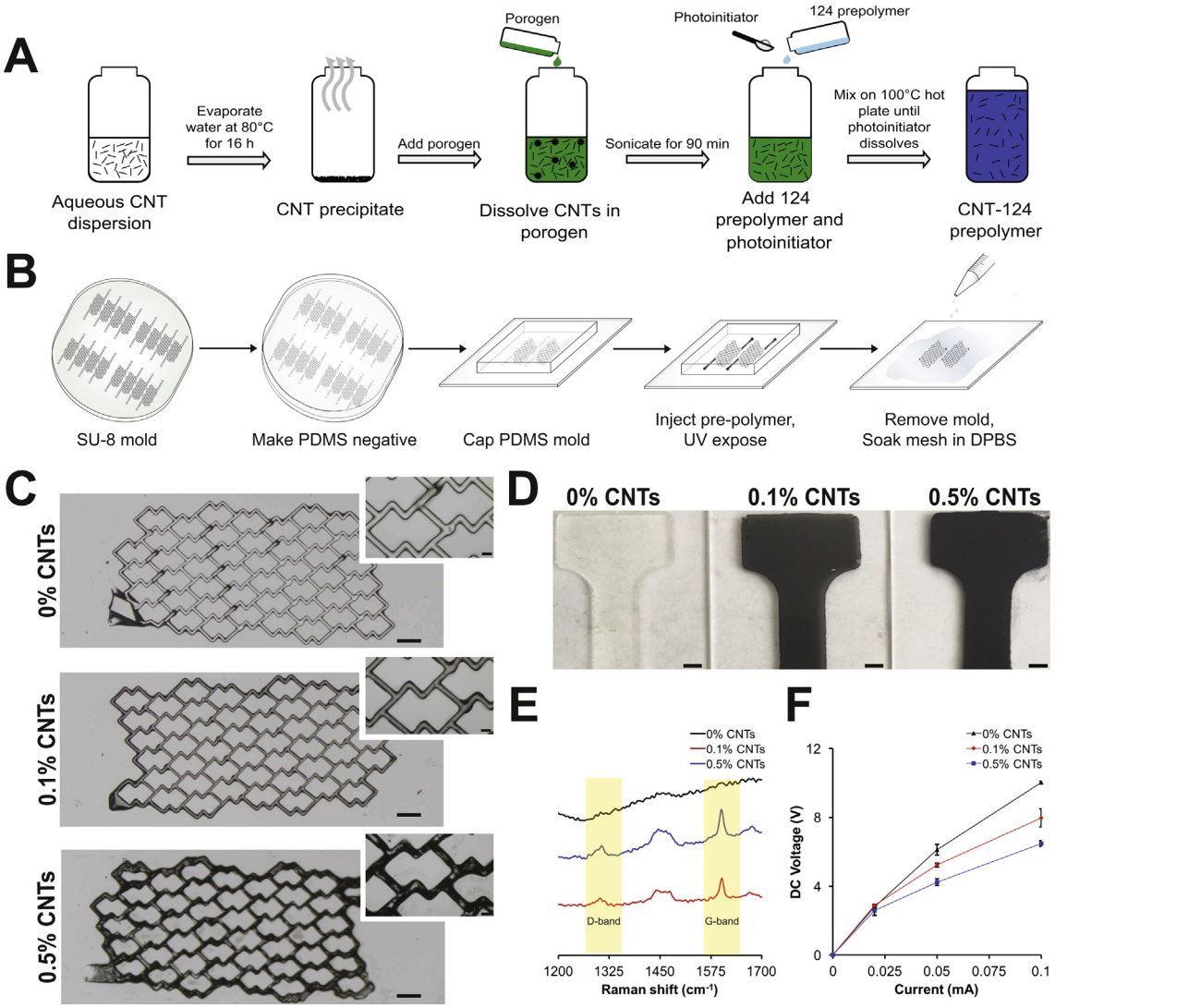

Fig. 1. Scaffold preparation and characterization (A) Schematic representation of 124 polymer-CNT prepolymer preparation. (B) Schematic representation of polymer molding into patch scaffolds for TE.(C) Bright field images presenting the moldability of the polymer materials in mesh structures containing 0, 0.1%, and 0.5% CNTs in 124 polymer (Scale bars: 400 μm (left) and 100 μm (top right)). (D) Polymer strips with increasing CNT concentration present visible darkening. (Scale bars: 200 μm) (E) Raman spectroscopy measurement of 124 polymer-CNT materials. Presence of D- and G-bands in the CNT containing samples is obvious in comparison to control. (F) Current-voltage (IV) curves for pure 124 polymer and 124 polymer-CNT materials.

conductivity was measured using an ionic conductivity meter (CM-25R, DKK-TOA Corporation, Japan) at ambient conditions.

2.5. Electron microscopy

Scanning electron microscopy (SEM) of porogen material was taken using a field emission SEM (JSM-6500F, JEOL, Japan) operated at 15 kV. SEM of 124 polymer materials was conducted using an ultra-high resolution field emission SEM (SU8230, Hitachi, Ontario Centre for the Characterization of Advanced Materials, Canada) at 10 kV. Polymer samples were prepared by soaking crosslinked strips for 24 h in DPBS, following by freezing and lyophilization (24 h). Transmission electron microscopy (TEM) images of CNTs were taken using a TEM (JEM-2100, JEOL, Japan) at 200 kV. For the TEM measurement, a drop of CNT dispersion was poured over a carbon-coated Cu TEM mesh grid and dried at RT.

2.6. Swelling measurement

Polymer swelling was quantified at room temperature (RT) using gravimetric method [26,27]. Dried polymer was weighed and covered with DPBS. The polymer weight was recorded at different times after carefully blotting the DPBS. Mass swelling ratio of polymers at the time (t) was calculated according to the following equation:

$$\text{Mass swelling ratio} = (W_t - W_d)/W_d * 100,$$

where W_t is the weight of wet polymer at the time t, W_d is the weight of dried polymer.

2.7. Degradation mass loss

Polymer degradation was assessed under pH 13 conditions. Polymer samples (approximately 50 mg) were crosslinked under UV light and placed in 20 mL glass vials of known mass. Ten milli-

liters of 0.1 M sodium hydroxide were added, the vial was sealed and placed under agitation at 37 °C. Samples (n = 3) were collected at 1, 2, and 3 h, washed twice with deionized distilled water, and dried under lyophilization for 24 h. The final mass was recorded then reported as a percentage of the initial mass that was lost. To confirm the leaching of PEGDM porogen in DPBS, the same experimental procedure was used with DPBS as the solution and final mass was assessed at 3 h.

2.8. Atomic force microscopy

An atomic force microscope (AFM; Bioscope Catalyst, Bruker, USA) was used to reveal the polymer surface modulus. Crosslinked polymer strips were observed under an inverted optical microscope (Nikon Eclipse-Ti, Japan). All measurements were made in air at RT. The Hertz model was selected to reveal the Young's modulus of polymer surfaces as described in previous work [28,29]. Calibration of cantilever spring constants was done prior to each measurement by quantifying power spectral density of thermal noise fluctuation of the cantilever. The Young's moduli were not significantly changed for AFM measurements at the same location.

2.9. Tensile testing

Tensile testing as conducted as described previously [25]. Briefly, 124 polymer-CNT prepolymer was injected into a polydimethylsiloxane (PDMS) mold for thin strips (length, 10 mm; width, 1.3 mm; thickness, 0.1 mm). Polymer samples were UV cured (3000 mJ/cm^2 using a mask aligner (Model 30 UV Light Source, OAI, USA)), then soaked in DPBS for porogen leaching (4 h). Tensile testing was conducted, under wet conditions, to failure using a Myograph (Kent Scientific). Bulk modulus was taken as the slope of the linear portion of a stress-strain relationship for each sample and toughness was calculated as the area under this curve.

2.10. Neonatal rat CM isolation

The digestion of neonatal rat heart tissue was done as previously described [30]. In brief, the heart of 1–2 day old neonatal Sprague-Dawley rats (Charles River, USA) was isolated and suspended in Ca^{2+}, Mg^{2+} free Hank's balanced salt solution (HBSS) (Gibco). The aorta and vena cava sections were then removed from the hearts. Subsequently, the hearts were cut into quarters and rinsed twice in cold HBSS. The heart pieces were then digested in a solution of 0.06% (w/v) trypsin (Sigma-Aldrich) in HBSS overnight (4 °C). The tissues were then digested in collagenase II (200 U/mL, Worthington, USA) in HBSS (37 °C) in five supplementary digestions of 4–8 min. Following digestion, cells were pre-plated for 45 min and non-adherent cells were collected for use as the rat CM population. Rat CMs were cultured in Dulbecco's modified Eagle's medium (Gibco) containing glucose (4.5 g/L), 10% (v/v) fetal bovine serum (FBS, Gibco), 1% (v/v) HEPES (100 U/mL, Gibco), and 1% (v/v) penicillin-streptomycin (100 mg/mL, Gibco).

2.11. Cardiac patch seeding

Cells were seeded on patches as described previously (Fig. 1B) [25,31]. In short, the mesh design (dimensions outlined in Fig. S5 of [25]) was generated using SU-8 photolithography techniques. From this, PDMS was poured to form a negative mold, which was capped with a glass slide and injected with prepolymer material. The scaffolds were crosslinked with UV light (6000 mJ/cm^2 exposed by a mask aligner (Model 30 UV Light Source, OAI, USA)), soaked in DPBS to leach out porogen and then sterilized with 70% ethanol. Scaffolds were then washed in DPBS, then coated with a 0.2% (wt) gelatin solution in DPBS for 3 h (37 °C) to promote cell attachment. Freshly isolated rat CMs were pelleted and mixed with Matrigel solution (4 °C, 1 million cells/ 1 μL Matrigel), and 2 μL of this mixture were pipetted onto each mesh surface. Meshes were kept at 37 °C for 2–3 min to facilitate the gelation process. Rat CM media (1 mL/well, 37 °C) was then added gently to the patches. Cell-laden patches were cultured for seven days, with media changes every 48 h. Viability of rat CMs was revealed by the incubation of tissues with CFDA-SE (C1157, Life Technologies, USA) and PI (P5366, Life Technologies, USA) in DPBS at 37 °C for 30 min. The immunofluorescent staining was conducted by first fixing tissues in 10% (w/v) formalin in DPBS at RT for 30 min. Cell permeation and blocking were then preformed in 10% FBS and 0.25% Triton X100 in DPBS for 1 h, followed by primary antibody incubation against sacromeric α-actinin (AB9465, Abcam) overnight at 4 °C. This was then incubated with secondary antibody, Donkey anti-mouse IgG (A21202, Life Technologies, USA) and Alexa Fluor® 660 phalliodin (A22285, Life Technologies, USA). Tissues were imaged using confocal microscopy (Olympus FV5-PSU (immunostaining) or Nikon A1R (viability staining), Canada). To quantify the cell viability, four different areas were selected in live-dead confocal images. The areas were far from the scaffold to avoid autofluorescence of scaffold in the cell viability quantification. Red and green intensities were measured using "Measure RGB" plugin in ImageJ software. The cell viability was then calculated based on the green intensity value divided by the sum of red and green intensities, as described previously [21,32,33].

2.12. Functional characterization

The contractility of cardiac patches was assessed with an S88X Grass Stimulator (Grass Technologies/AstroMed Inc., USA) as described previously [31,32]. Patches were put in a stimulation chamber seven days post seeding and subjected to a biphasic square (Frequency; 1 Hz, pulse duration; 2-ms). The excitation threshold (ET, V/cm) was assessed with voltage increase from 0 V at 0.1 V increments until the tissue construct was visibly paced in agreement with the stimulator outputs. Then, the maximum capture rate (MCR, Hz) was tested by doubling the ET output voltage and increasing the frequency of stimulation (0.1 Hz increments) until the constructs could no longer pace with the stimulator outputs.

2.13. Statistical methods

Error bars seen in figures present data as average ± standard deviation. Each experiment was conduct with a minimum of three replicates. Statistical analysis was conducted using SigmaPlot 12. Statistically significant differences were analyzed using one-way ANOVA followed by a Tukey-Kramer test at a significance of $p < 0.05$.

3. Results

3.1. Development of 124 polymer-CNT materials

124 polymer-CNT materials were developed by first mixing CNT powder with porogen with sonication, then mixing with 124 prepolymer to disperse CNTs within the material (Fig. 1A). The lower viscosity of porogen allowed for easier dispersion of CNTs by sonication in contrast to direct dispersion in 124 prepolymer. It has been shown previously that PEGDM is completely miscible with 124 prepolymer, allowing the dispersion of suspended CNTs along with porogen [25]. Following mixing, Irgacure 2959 photoinitiator was easily combined under heat to activate the UV crosslinkable

functionality of the materials. Prepolymer materials with CNT content appeared visibly translucent, with increasing black color corresponding to increased CNT concentration.

Moldability of 124 polymer-CNT materials was demonstrated through construction of mesh structures with micron-sized features. Through conventional photolithography techniques, a SU-8 master mold (Nominal height, 100 μm) was developed and used to generate PDMS negative molds for prepolymer injection and shaping (Fig. 1B) [25,31]. Following exposure to UV light, 124 polymer-CNT materials with 0%, 0.1% and 0.5% CNTs maintained their molded shape upon removal of the PDMS mold and release from the glass slide in DPBS solution (Fig. 1C). With immersion in DPBS, porogen leaches out of the polymer bulk, while the CNTs remained visibly entrapped within the crosslinked mesh structure, consistent with previous studies (Fig. 1C, top right) [25,34]. Porogen leaching was assessed by mass loss testing following 3 h of immersion in DPBS, where material containing 0%, 0.1% and 0.5% CNTs exhibited 33.4 ± 1.5%, 35.2 ± 2.5%, and 33.7 ± 2.4% mass loss, respectively. On a macroscale, visible darkening is observed with increasing the CNT content (Fig. 1D).

Raman spectroscopy was used to confirm high quality of CNTs within 124 polymer-CNT constructs (Fig. 1E). D-bands were observed at 1302 and 1306 cm^{-1} for 124 polymer-0.1% CNTs and 124 polymer-0.5% CNTs, respectively, while G-bands were recorded at 1602 and 1601 cm^{-1} for 124 polymer-0.1% CNTs and 124 polymer-0.5% CNTs, respectively. The intensity ratios of G-band to D-band were 1.35 and 1.33 for 124 polymer-0.1% CNTs and 124 polymer-0.5% CNTs, respectively. These ratios are close to that reported for pristine multi-walled CNTs [35,36] indicating high quality of CNTs inside polymer networks. The D-band and G-band were not detectable in the Raman spectroscopy of pure 124 polymer. Notable peaks at ~1450 and 1660 cm^{-1} in the Raman spectra of polymers were attributed to C—H and C═C bands, respectively [37].

124 polymer-CNT materials containing 0%, 0.1% and 0.5% CNTs were assessed for electrical conductivity (Fig. 1F). Voltage output (V) was recorded with increasing electrical current (I), demonstrating material resistance (R) according to V = RI. A trend of decreasing resistance was observed from pure 124 polymer material ($R = 98.6 \pm 1.3$ kΩ, $R^2 = 0.98$) to those with 0.1% CNTs ($R = 76.2 \pm 5.3$ kΩ, $R^2 = 0.96$) and 0.5% CNTs ($R = 60.9 \pm 1.0$ kΩ, $R^2 = 0.94$), indicating increased conductivity with higher weight percentage of CNTs. Furthermore, we measured the solution's conductivity of CNTs suspended in porogen. The CNT-porogen mixture had a solution's ionic conductivity of 0.08 ± 0.01 mS/m, compared to a value of 0.06 ± 0.01 mS/m for porogen without CNTs and 0.06 ± 0.01 mS/m for distilled water.

High magnification imaging of CNTs and 124 polymer-CNT materials was performed using SEM and TEM. Comparison of CNTs in distilled water (Fig. 2A) to those in porogen (Fig. 2B) with SEM imaging shows an increased brightness around CNT structures. The structure of a single CNT was clearly observed through TEM imaging (Fig. 2C). Single CNTs were also observed upon mixing with porogen, as expected (Fig. 2D). Upon incorporation into the polymer, CNTs were clearly detectable in the composites (Fig. 2F) in comparison to pristine, CNT-free polymers (Fig. 2E).

3.2. Physical properties of polymers

Bulk and surface mechanical properties of 124 polymer-CNT materials were assessed. CNT containing materials presented comparable elongation with 124 polymer under manual stretch (Fig. 3A). Bulk modulus measurements showed a higher modulus under wet conditions for pure 124 polymer material (3.6 ± 0.6 MPa) in comparison to 0.1% CNT (2.2 ± 0.3 MPa) and 0.5% CNT (1.6 ± 0.7 MPa) materials (Fig. 3B). The toughness for pure 124 polymer material was 105 ± 18 MJ m^{-3} while those with 0.1% and 0.5% CNT contents were 76 ± 11 MJ m^{-3} and 51 ± 18 MJ m^{-3}, respectively, and were consistent with the toughness of other elastomers [38–40]. In contrast, using AFM, surface moduli of materials with 0%, 0.1% and 0.5% CNT content were compared (Fig. 3C). Those with 0.5% CNTs presented a significantly higher surface modulus (13.6 ± 0.9 MPa) than 0.1% (3.3 ± 0.1 MPa) and 0% CNT (2.9 ± 0.1 MPa) materials. The ability for cyclic loading of materials with 0.5% CNTs was qualitatively comparable to pure 124 polymer control (Supplementary Movie 1).

Swelling properties of 124 polymer-CNT materials were assessed over time in DPBS. Mass swelling of materials was done with 0%, 0.1% and 0.5% CNTs over time (Fig. 3D). With increasing CNT content we observed increased swelling on the mass basis, with peak values of 2.4 ± 2.7%, 12.8 ± 4.4%, and 36.8 ± 2.7% for 0%, 0.1% and 0.5% CNT content materials, respectively. With 0% and 0.1% CNTs we observed a decline in swelling amount after 1 h, whereas 0.5% CNTs presented an increasing trend over time. It should be noted that in this process porogen (initial concentration, 50%) leached from the materials leaving a porous structure to facilitate DPBS uptake into the polymer bulk. A negative value for the mass swelling percentage is indicative of a decreased swelling volume of water in comparison to porogen (density: 1.03 g/mL).

124 polymer-CNT materials were assessed for mass loss under accelerated conditions (0.1 M NaOH) to determine the potential effect of CNTs on degradability (Fig. 3E) [34]. All three materials completely degraded over a 3 h period, where a slightly increased rate was observed in CNT containing samples. Some of the initial mass loss in all materials can be attributed to the solubility of PEGDM porogen. CNT containing materials presented visible darkening in the vial supernatant at each time point, suggesting the release of CNTs into the aqueous environment and presenting the reversible entrapment in the polymer bulk.

3.3. In vitro cardiac tissue constructs

To assess the application of conductive 124 polymer-CNT materials in cardiac tissue regeneration, we used an optimum scaffold design for developing cardiac constructs and utilized 124 polymer-CNT materials as the scaffold material [25,31]. Mesh designs were molded and sterilized for seeding with freshly isolated rat CMs. Seven days post seeding, cells showed tissue compaction around the scaffold struts on constructs with 0%, 0.1% and 0.5% CNT content (Fig. 4A). Fabricated cardiac tissues showed consistent and spontaneous beating at day 4 in 124 polymer-CNT scaffolds while it typically took until day 6 to observe a comparable beating in scaffold constructs of pure 124 polymer material. Side by side comparison of scaffolds at day 4 (Supplementary Movie 2) and day 6 (Supplementary Movie 3) demonstrated earlier spontaneous beating in 124 polymer-CNT materials. Furthermore, 0.5% CNT constructs presented a more coordinated beating through visual observation than 0% and 0.1% CNT containing scaffolds. Tissue constructs exhibited comparable viability at day 7 when assessed visually with staining for CFSA-SE (green, live cells) and PI (red, dead cells) (Fig. 4B). It should be noted that the 124 polymer material presents autofluorescence in the red channel, and this intensity was decreased with the addition of CNTs. Higher magnification excerpts show a low number of dead cells (red) in the tissue area adjacent to the autofluorescent scaffold. Viability quantification using pixel color presented no significant difference between the material groups (Fig. 4D).

With functional characterization, scaffolds constructs with 0.5% CNTs exhibited a significantly lower ET (3.6 ± 0.8 V/cm) than materials with 0% (5.1 ± 0.8 V/cm) and 0.1% (5.0 ± 0.7 V/cm) CNTs (Fig. 4E). There were no statistically significant differences observed in MCR for these tissues (Fig. 4F). Immunofluorescent

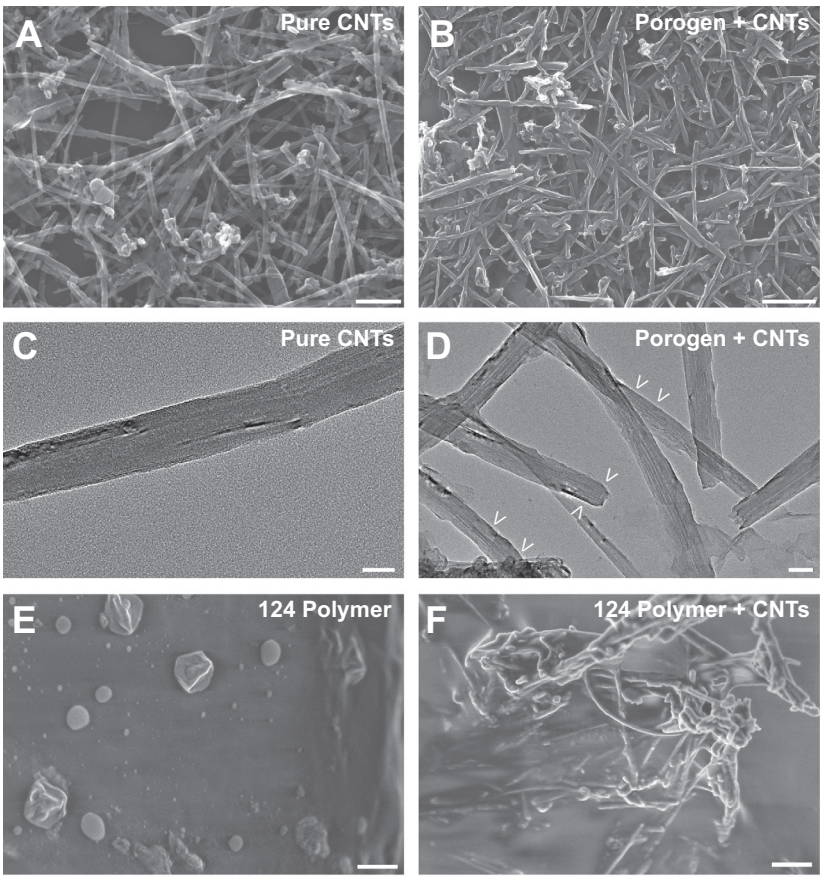

Fig. 2. High magnification images of CNTs and CNT-124 polymers (A, B) SEM (Scale bars: 1 μm) and (C, D) TEM images (Scale bars: 25 nm (left), 50 nm (right)) of CNTs dispersed in water (A and C) and porogen (B and D). Arrows in (D) present a bright outline around CNTs indicative of nanotube wrapping by the porogen material (E, F) SEM images of UV-crosslinked polymer constructs with 0.5% CNT content (F) in comparison to blank polymer control (E) (Scale bars: 500 nm).

staining of tissue constructs was performed at day 7, with staining for sacromeric α-actinin (green) and F-actin (red) (Fig. 5A). Characteristic cross striations of organized cardiac tissue were evident in tissue constructs with 0%, 0.1% and 0.5% CNTs, as presented in higher magnification images of both channels (Fig. 5B) and the isolated green channel (Fig. 5C).

4. Discussion

Given that native cardiac tissues exhibit high flexibility, electrical conductance, and contractility, desired scaffolds in cardiac TE should present high electrical conductivity and flexibility. 124 polymer-CNT materials were readily generated through first dispersing CNTs in porogen and then combining them with 124 prepolymer for molding into intricate shapes. Our previous microscale TE works relied on porogen content to improve material processability for molding through a decrease in prepolymer viscosity, while also inducing porosity in the scaffold backbone [31,34]. Herein, we utilized these advantages to develop a carrier of CNT incorporation. Thereby, we were able to combine the beneficial properties of high conductivity and high elasticity in a single material. Porogen acts as an ideal dispersant for CNTs as it is non-cytotoxic [25,31,34,41], miscible in 124 prepolymer, soluble in DPBS for simple leaching post-processing and has low detrimental effect on PDMS molds. The leaching process presented over 30% mass loss within 3 h of immersion in DPBS, was consistent with relatively fast porogen removal with the maintenance of polymer structure as described in previous studies [41]. A similar strategy could be used to incorporate CNTs inside other polymeric biomaterials, such as poly(L-lactic acid) [42] and polycaprolactone [43] with porogen as the CNT carrier.

It has previously been demonstrated that incorporation of CNTs into polymer materials induces inherent conductivity [23,44]. We have demonstrated similar characteristics; with increased CNT content in the material the resistive properties decreased, suggesting improved material conductivity (Fig. 1F). The improved conductivity could be a direct result of CNT conductivity or also improved ion penetration into the bulk scaffold material, resultant of increased chelating properties in 124 polymer-CNT materials. As we previously described, 124 polymer is advantageous for its two-step preparation process, wherein we first synthesize a prepolymer that can simply be molded into intricate designs through material injection and then crosslinked under UV light to give an elastomeric robust construct [25]. Furthermore, its elastic properties are ideal for cardiac TE, exhibiting a tunable Young's modulus that falls within the range of human adult myocardium (diastole: 10–20 kPa, systole: 200–300 kPa) to support the contractile behavior of constructs [25,45–48]. The contractile nature of cardiac tissue necessitates a material that can withstand cyclic elongation and relaxation without tissue inhibition. With the incorporation of CNTs, 124 polymer maintained this functionality (Fig. 1C), suggesting a distinct advantage to this material in microscale fabrication through the material injection.

High-resolution imaging (Fig. 2) supports the ability of our methods to effectively distribute CNTs within porogen and in succession generate 124 polymer-CNT. The negligible differences between solution's ionic conductivity in porogen-CNTs to controls suggest little charge interaction between porogen and dispersed

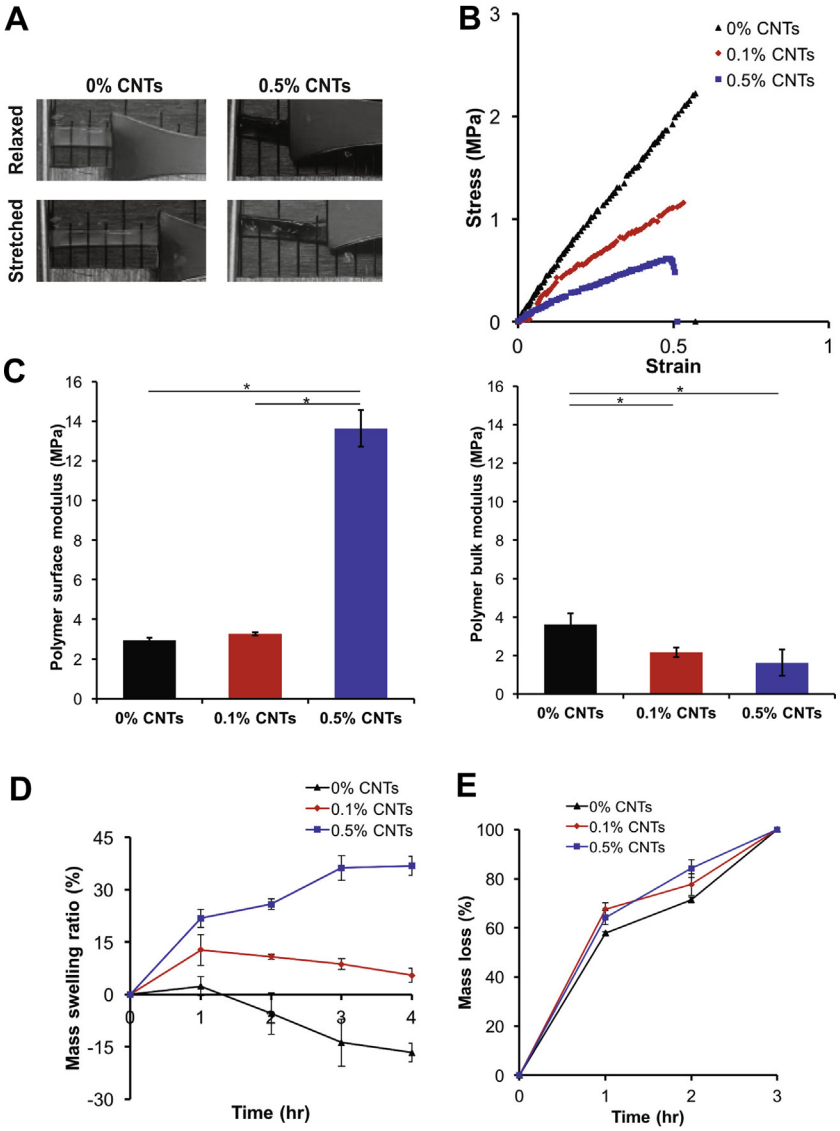

Fig. 3. Physical properties of 124 polymer-CNT materials. (A) Demonstration of elastic stretch in material with 0% (left) and 0.5% (right) CNT content (Scale in mm). (B) Stress-strain curve comparing materials with 0%, 0.1% and 0.5% CNT content. (C) Surface and bulk polymer moduli of materials (*p<0.05). (D) Quantification of swelling by mass suggests increased water uptake with higher CNT content. (E) Accelerated degradation (0.1 M NaOH) of CNT-124 polymer materials.

CNTs. Therefore, it seems that spatial wrapping of CNTs using porogen is the main mechanism of CNT dispersion in porogen. When comparing SEM images of CNTs dispersed in porogen to pristine CNTs we observed a bright outline, which further suggests the wrapping of porogen around CNTs. The presence of porogen around individual CNTs was also obvious in the TEM image of porogen-CNTs (Fig. 2D). As such, CNTs were stabilized in the porogen solution and they did not precipitate, suggesting the suspension of the nanotubes through steric stabilization. The proposed mechanism was also reported in the case of CNT dispersion in gelatin methacryloyl hydrogel [49].

Incorporation of CNTs into polymers demonstrated increased swelling compared to pure polymer controls on a mass basis. In CNT containing materials we observed a significantly positive mass swelling ratio, suggesting an increased water uptake into vacated pores. This suggests that CNTs play a role in maintaining microporosity within the material, such that the tubes could maintain pore volume and allow water entry with greater ease. The discrepancy in surface and bulk moduli further explains these observations. It has been previously reported that CNTs tend to increase the stiffness of polymers [50,51]. This is supported in our measurements of surface moduli with AFM, where 0.5% CNT materials exhibited a modulus 10 times higher than that of pure 124 polymer material. This trend was contrasted with tensile property measurements of the polymer bulks, where increased CNT content presented a decreased modulus and material toughness. We also attribute this to interference of CNTs with the UV crosslinking polymer. There is a visible increase in opacity with CNT content (Fig. 1D), which would interfere with the ability of UV light to initiate radical polymerization through the thickness of the polymer bulk. In addition, CNTs can absorb UV light, decreasing the energy transferred into chemical crosslinking [52]. In agreement with our results, we have previously shown the UV energy exposed to 124 polymer has a direct effect on its modulus [25]. Therefore, this further suggests that CNT content in UV crosslinked 124 polymer constructs helps to maintain lower bulk modulus of the polymer due to a lower crosslinking density. The dispersion and absorption of UV light by CNTs most likely minimize the formation of crosslinks developed through the activation of photoinitiator radicals. With fewer crosslinks, polymer chains are more mobile within the poly-

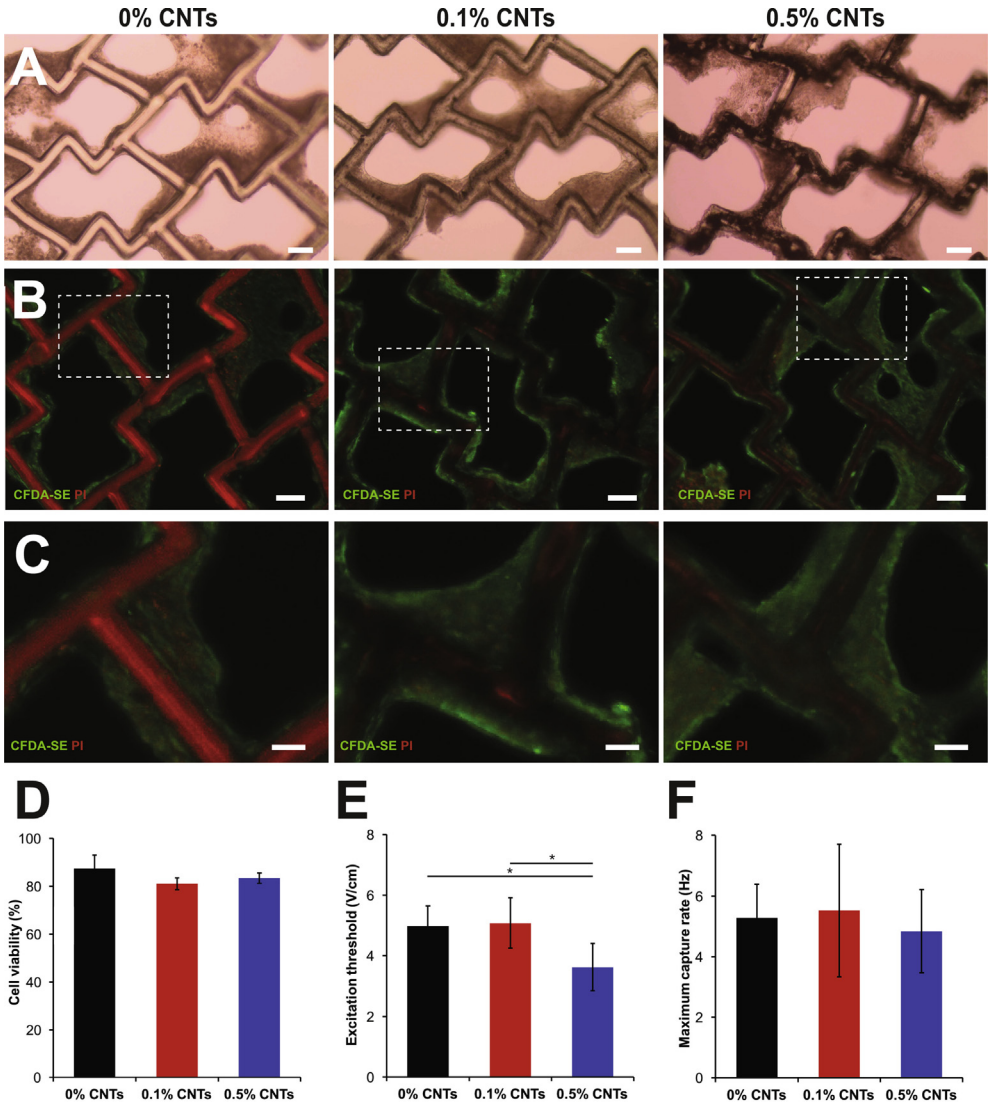

Fig. 4. Composite scaffolds in cardiac tissue engineering. (A–C) Images of rat cardiac tissue constructs with 124 polymer-CNT scaffolds containing 0.1% and 0.5% CNTs compared to pure polymer scaffolds. (A) Bright field images of polymers seeded with rat CMs at day 7 of culture demonstrate tissue compaction around scaffold struts (Scale bars: 100 μm). (B) Tissues were imaged for viability with live/dead staining assay (Live cells: green, dead cells: red), where the scaffold exhibits autofluorescence in the red channel (Scale bars: 100 μm). (C) High magnification excerpts demonstrate the wrapping of viable cells around scaffold struts (Scale bars: 50 μm). (D) Cell viability quantification of live-dead images present no difference between material groups. (E and F) Comparison of excitation threshold (E) and maximum capture rate (F) suggest improved tissue properties with 0.5% CNTs in polymer scaffolds in comparison to pure polymer controls (*$p<0.05$). (For interpretation of the references to colour in this figure legend, the reader is referred to the web version of this article.)

mer bulk, leading to a decreased bulk modulus in comparison to a blank control subject to the same crosslinking conditions. This is supported by the increased rate of degradation in the CNT containing materials when compared to 0% CNT polymer. With fewer radical crosslinks, hydrolytic degradation would be more favorable. This can also explain the increased swelling observed in CNT-124 polymer materials, as polymer chain rearrangement is easier in these materials to support water uptake. Overall, the tensile moduli observed are advantageous in the context of cardiac TE applications, as they fall within the range of values observed in human adult myocardium. These values could be tuned, as we reported previously, to reach a desired modulus [25].

124 polymer-CNT materials demonstrated functional improvement of cardiac TE constructs. In comparison of the ET for scaffolds with 0.5% CNTs to those with 0.1% and 0% CNTs (Fig. 4E) there was a significant decrease, suggesting significantly positive effect of CNTs on the tissue maturity. Furthermore, qualitative observation suggested stronger coordinated beating in the CNT containing scaffolds and earlier initiation of spontaneous beating of CMs. The interconnectivity among CNTs in scaffolds with 0.5% CNT content was higher than 0.1% CNT materials (Fig. 1C, 4A), which supports the findings of increased electrical conductivity and improved tissue maturation due to more facile current propagation in 0.5% CNT scaffolds.

Comparison of viability (Fig. 4B–D) suggest that CNT addition to 124 polymer scaffolds does not induce cytotoxic effects, in line with our previous findings on 124 polymer material [25]. This also supports low toxicity of CNTs can be achieved while harnessing their benefits in biomedical applications [53–56]. The presence of cross striations in immunostained tissues further confirmed the ability for organized cardiac tissues to form on 124 polymer-CNT materials (Fig. 5). These materials present an exciting option for use in cardiac TE, suggesting the improved conductance of scaffolds and increased electrical signaling between CMs, allowing for more rapid tissue organization and maturation. This difference could be further pronounced if cells were subject to previously

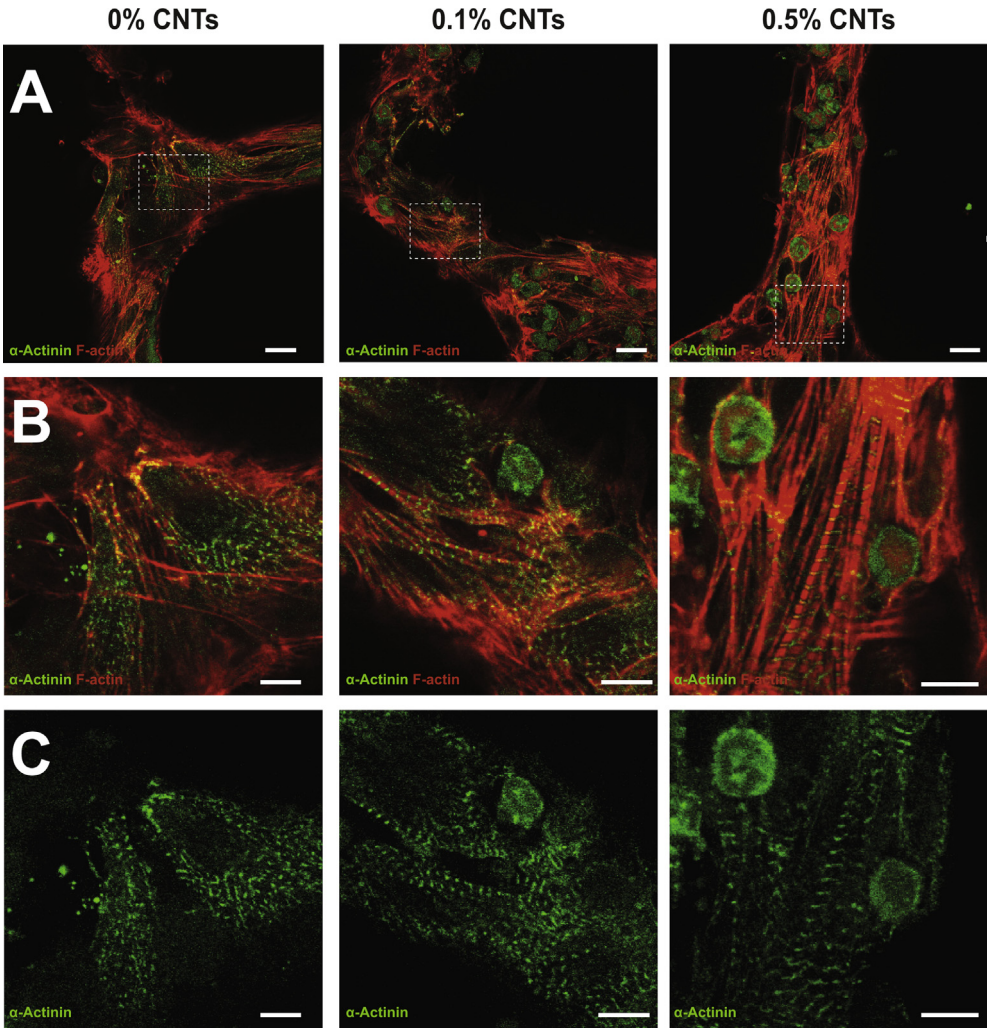

Fig. 5. Formation of organized cardiac tissue constructs. (A) Immunostaining of cardiac tissue constructs 7 days post seeding with sacromeric alpha actinin (green) and F-actin (red) (Scale bars: 20 μm). (B and C) High magnification image shows characteristic cross-striations of organized cardiac tissue (Scale bars: 10 μm). (For interpretation of the references to colour in this figure legend, the reader is referred to the web version of this article.)

published maturation protocols that utilize strict changes in electrical stimulation frequencies to induce tissue maturity [57]. These materials build on the advantages of 124 polymer giving a versatile biomaterial for microfabricated tissue engineered constructs.

5. Conclusions

Herein, we described the generation of CNT-124 polymer materials through the suspension of CNTs in PEGDM porogen and combination of this solution with 124 prepolymer. These materials showed the ability to be molded into complex shapes and cross-linked to give an elastomeric scaffold structure for cardiac TE applications. Through functional assessment, we observed improved tissue maturity on scaffolds with CNT content, suggesting the applicability of this polymer to make functional engineered tissue constructs.

Author contribution

S.A., L.D.H., and M.R. conceived the idea, designed the experiments, and analyzed the results. S.A. and L.D.H. performed the experiments and analyzed the results. S.A. tested the electrical conductivity, Raman spectroscopy, and material swelling. L.D.H. performed polymer synthesis and CNT-124 material preparation, cardiac patch culture, tensile testing, and imaging. M.E. functionalized the CNTs and prepared highly stable aqueous CNT dispersion, measured solution's ionic conductivity of samples, and performed SEM and TEM microscopy. B.Y. and N.S. contributed to experiments and analysis. Z.X. and Y.S. performed the AFM measurements. S.A. and L.D.H. wrote the manuscript. M.R. supervised the entire project. S.A. and L.D.H. contributed equally to the work. All authors read the manuscript, commented on it, and approved its content.

Acknowledgements

The authors would like to thank Dr. Boyang Zhang (University of Toronto, Canada) for guidance on *in vitro* cardiac patch seeding and confocal microscopy. L.D.H is supported by CIHR Canada Graduate Scholarships-Masters and CIHR Vanier Canada Graduate Scholarships. This work is funded by the NSERC Steacie Fellowship to M.R., Canadian Institutes of Health Research (CIHR) Operating Grants (MOP-126027 and MOP-137107), NSERC Discovery Grant (RGPIN 326982-10) and McLean Award.

Appendix A. Supplementary data

Supplementary data associated with this article can be found, in the online version, at http://dx.doi.org/10.1016/j.actbio.2016.12.009.

References

[1] D. Mozaffarian, E.J. Benjamin, A.S. Go, D.K. Arnett, M.J. Blaha, M. Cushman, S.R. Das, S. de Ferranti, J.-P. Després, H.J. Fullerton, V.J. Howard, M.D. Huffman, C.R. Isasi, M.C. Jiménez, S.E. Judd, B.M. Kissela, J.H. Lichtman, L.D. Lisabeth, S. Liu, R. H. Mackey, D.J. Magid, D.K. McGuire, E.R. Mohler III, C.S. Moy, P. Muntner, M.E. Mussolino, K. Nasir, R.W. Neumar, G. Nichol, L. Palaniappan, D.K. Pandey, M.J. Reeves, C.J. Rodriguez, W. Rosamond, P.D. Sorlie, J. Stein, A. Towfighi, T.N. Turan, S.S. Virani, D. Woo, R.W. Yeh, M.B. Turner, Heart disease and stroke statistics-2016 update: a report from the American heart association, Circulation 132 (2015), http://dx.doi.org/10.1161/CIR.0000000000000350.

[2] E. Braunwald, The war against heart failure: the Lancet lecture, Lancet 385 (2015) 812–824.

[3] A. Pahnke, G. Conant, L.D. Huyer, Y. Zhao, N. Feric, M. Radisic, The role of Wnt regulation in heart development, cardiac repair and disease: a tissue engineering perspective, Biochem. Biophys. Res. Commun. 473 (2016) 698–703.

[4] L.D. Huyer, M. Montgomery, Y. Zhao, Y. Xiao, G. Conant, A. Korolj, M. Radisic, Biomaterial based cardiac tissue engineering and its applications, Biomed. Mater. 10 (2015) 034004.

[5] S. Ahadian, S. Ostrovidov, V. Hosseini, H. Kaji, M. Ramalingam, H. Bae, A. Khademhosseini, Electrical stimulation as a biomimicry tool for regulating muscle cell behavior, Organogenesis 9 (2013) 87–92.

[6] N.Y. Liaw, W.-H. Zimmermann, Mechanical stimulation in the engineering of heart muscle, Adv. Drug Del. Rev. 96 (2016) 156–160.

[7] C. Alperin, P.W. Zandstra, K.A. Woodhouse, Polyurethane films seeded with embryonic stem cell-derived cardiomyocytes for use in cardiac tissue engineering applications, Biomaterials 26 (2005) 7377–7386.

[8] G.C. Engelmayr, M. Cheng, C.J. Bettinger, J.T. Borenstein, R. Langer, L.E. Freed, Accordion-like honeycombs for tissue engineering of cardiac anisotropy, Nat. Mater. 7 (2008) 1003–1010.

[9] M. Shachar, O. Tsur-Gang, T. Dvir, J. Leor, S. Cohen, The effect of immobilized RGD peptide in alginate scaffolds on cardiac tissue engineering, Acta Biomater. 7 (2011) 152–162.

[10] P. Akhyari, P.W.M. Fedak, R.D. Weisel, T.-Y.J. Lee, S. Verma, D.A.G. Mickle, R.-K. Li, Mechanical stretch regimen enhances the formation of bioengineered autologous cardiac muscle grafts, Circulation 106 (2002) I137–1142.

[11] S. Pok, J.D. Myers, S.V. Madihally, J.G. Jacot, A multilayered scaffold of a chitosan and gelatin hydrogel supported by a PCL core for cardiac tissue engineering, Acta Biomater. 9 (2013) 5630–5642.

[12] E. Rosellini, C. Cristallini, N. Barbani, G. Vozzi, P. Giusti, Preparation and characterization of alginate/gelatin blend films for cardiac tissue engineering, J. Biomed. Mater. Res. A 91 (2009) 447–453.

[13] D.A. Stout, Recent advancements in carbon nanofiber and carbon nanotube applications in drug delivery and tissue engineering, Curr. Pharm. Des. 21 (2015) 2037–2044.

[14] S. Ahadian, S. Yamada, J. Ramón-Azcón, M. Estili, X. Liang, K. Nakajima, H. Shiku, A. Khademhosseini, T. Matsue, Hybrid hydrogel-aligned carbon nanotube scaffolds to enhance cardiac differentiation of embryoid bodies, Acta Biomater. 31 (2016) 134–143.

[15] S. Ahadian, Y. Zhou, S. Yamada, M. Estili, X. Liang, K. Nakajima, H. Shiku, T. Matsue, Graphene induces spontaneous cardiac differentiation in embryoid bodies, Nanoscale 8 (2016) 7075–7084.

[16] X. Ding, H. Liu, Y. Fan, Graphene-based materials in regenerative medicine, Adv. Healthcare Mater. 4 (2015) 1451–1468.

[17] S.R. Shin, S.M. Jung, M. Zalabany, K. Kim, P. Zorlutuna, S.B. Kim, M. Nikkhah, M. Khabiry, M. Azize, J. Kong, K.-T. Wan, T. Palacios, M.R. Dokmeci, H. Bae, X. Tang, A. Khademhosseini, Carbon-nanotube-embedded hydrogel sheets for engineering cardiac constructs and bioactuators, ACS Nano 7 (2013) 2369–2380.

[18] V. Martinelli, G. Cellot, F.M. Toma, C.S. Long, J.H. Caldwell, L. Zentilin, M. Giacca, A. Turco, M. Prato, L. Ballerini, L. Mestroni, Carbon nanotubes promote growth and spontaneous electrical activity in cultured cardiac myocytes, Nano Lett. 12 (2012) 1831–1838.

[19] S.R. Shin, C. Zihlmann, M. Akbari, P. Assawes, L. Cheung, K. Zhang, V. Manoharan, Y.S. Zhang, M. Yüksekkaya, K.-T. Wan, M. Nikkhah, M.R. Dokmeci, X. Tang, A. Khademhosseini, Reduced graphene oxide-GelMA hybrid hydrogels as scaffolds for cardiac tissue engineering, Small 12 (2016) 3677–3689.

[20] N. Annabi, S.R. Shin, A. Tamayol, M. Miscuglio, M.A. Bakooshli, A. Assmann, P. Mostafalu, J.Y. Sun, S. Mithieux, L. Cheung, X. Tang, A.S. Weiss, A. Khademhosseini, Highly elastic and conductive human-based protein hybrid hydrogels, Adv. Mater. 28 (2016) 40–49.

[21] M. Kharaziha, S.R. Shin, M. Nikkhah, S.N. Topkaya, N. Masoumi, N. Annabi, M.R. Dokmeci, A. Khademhosseini, Tough and flexible CNT-polymeric hybrid scaffolds for engineering cardiac constructs, Biomaterials 35 (2014) 7346–7354.

[22] Y. Liu, J. Lu, G. Xu, J. Wei, Z. Zhang, X. Li, Tuning the conductivity and inner structure of electrospun fibers to promote cardiomyocyte elongation and synchronous beating, Mater. Sci. Eng. C 69 (2016) 865–874.

[23] D.A. Stout, B. Basu, T.J. Webster, Poly(lactic-co-glycolic acid): carbon nanofiber composites for myocardial tissue engineering applications, Acta Biomater. 7 (2011) 3101–3112.

[24] S. Marchesan, S. Bosi, A. Alshatwi, M. Prato, Carbon nanotubes for organ regeneration: an electrifying performance, Nano Today 11 (2016) 398–401.

[25] L.D. Huyer, B. Zhang, A. Korolj, M. Montgomery, S. Drecun, G. Conant, Y. Zhao, L. Reis, M. Radisic, Highly elastic and moldable polyester biomaterial for cardiac tissue engineering applications, ACS Biomater. Sci. Eng. 2 (2016) 780–788.

[26] H. Jiankang, L. Dichen, L. Yaxiong, Y. Bo, Z. Hanxiang, L. Qin, L. Bingheng, L. Yi, Preparation of chitosan–gelatin hybrid scaffolds with well-organized microstructures for hepatic tissue engineering, Acta Biomater. 5 (2009) 453–461.

[27] Z. Li, M. Tang, J. Dai, T. Wang, R. Bai, Effect of multiwalled carbon nanotube-grafted polymer brushes on the mechanical and swelling properties of polyacrylamide composite hydrogels, Polymer 85 (2016) 67–76.

[28] S. Ahadian, R.B. Sadeghian, S. Yaginuma, J. Ramón-Azcón, Y. Nashimoto, X. Liang, H. Bae, K. Nakajima, H. Shiku, T. Matsue, K.S. Nakayama, A. Khademhosseini, Hydrogels containing metallic glass sub-micron wires for regulating skeletal muscle cell behaviour, Biomater. Sci. 3 (2015) 1449–1458.

[29] H. Liu, Q. Tan, W.R. Geddie, M.A.S. Jewett, N. Phillips, D. Ke, C.A. Simmons, Y. Sun, Biophysical characterization of bladder cancer cells with different metastatic potential, Cell Biochem. Biophys. 68 (2014) 241–246.

[30] M. Radisic, H. Park, H. Shing, T. Consi, F.J. Schoen, R. Langer, L.E. Freed, G. Vunjak-Novakovic, Functional assembly of engineered myocardium by electrical stimulation of cardiac myocytes cultured on scaffolds, Proc. Natl. Acad. Sci. U.S.A. 101 (2004) 18129–18134.

[31] B. Zhang, M. Montgomery, L.D. Huyer, A. Korolj, M. Radisic, Platform technology for scalable assembly of instantaneously functional mosaic tissues, Sci. Adv. 1 (2015) e1500423.

[32] R.K. Iyer, L.L.Y. Chiu, M. Radisic, Microfabricated poly(ethylene glycol) templates enable rapid screening of triculture conditions for cardiac tissue engineering, J. Biomed. Mater. Res. A 89 (2009) 616–631.

[33] L.A. Reis, L.L.Y. Chiu, Y. Liang, K. Hyunh, A. Momen, M. Radisic, A peptide-modified chitosan-collagen hydrogel for cardiac cell culture and delivery, Acta Biomater. 8 (2012) 1022–1036.

[34] B. Zhang, M. Montgomery, M.D. Chamberlain, S. Ogawa, A. Korolj, A. Pahnke, L. A. Wells, S. Massé, J. Kim, L. Reis, A. Momen, S.S. Nunes, A.R. Wheeler, K. Nanthakumar, G. Keller, M.V. Sefton, M. Radisic, Biodegradable scaffold with built-in vasculature for organ-on-a-chip engineering and direct surgical anastomosis, Nature Mater. 15 (2016) 669–678.

[35] V. Datsyuk, M. Kalyva, K. Papagelis, J. Parthenios, D. Tasis, A. Siokou, I. Kallitsis, C. Galiotis, Chemical oxidation of multiwalled carbon nanotubes, Carbon 46 (2008) 833–840.

[36] M. Estili, A. Kawasaki, Y. Sakka, Highly concentrated 3D macrostructure of individual carbon nanotubes in a ceramic environment, Adv. Mater. 24 (2012) 4322–4326.

[37] M. Skrifvars, P. Niemelä, R. Koskinen, O. Hormi, Process cure monitoring of unsaturated polyester resins, vinyl ester resins, and gel coats by Raman spectroscopy, J. Appl. Polym. Sci. 93 (2004) 1285–1292.

[38] M.Z. Seyedin, J.M. Razal, P.C. Innis, G.G. Wallace, Strain-responsive polyurethane/PEDOT:PSS elastomeric composite fibers with high electrical conductivity, Adv. Funct. Mater. 24 (2014) 2957–2966.

[39] Z. Chen, H. Lu, Constructing sacrificial bonds and hidden lengths for ductile graphene/polyurethane elastomers with improved strength and toughness, J. Mater. Chem. 22 (2012) 12479–12490.

[40] R. Casalini, R. Bogoslovov, S.B. Qadri, C.M. Roland, Nanofiller reinforcement of elastomeric polyurea, Polymer 53 (2012) 1282–1287.

[41] R.A. Hoshi, S. Behl, G.A. Ameer, Nanoporous biodegradable elastomers, Adv. Mater. 21 (2009) 188–192.

[42] Y.S. Nam, J.J. Yoon, T.G. Park, A novel fabrication method of macroporous biodegradable polymer scaffolds using gas foaming salt as a porogen additive, J. Biomed. Mater. Res. 53 (2000) 1–7.

[43] M.J. Mondrinos, R. Dembzynski, L. Lu, V.K.C. Byrapogu, D.M. Wootton, P.I. Lelkes, J. Zhou, Porogen-based solid freeform fabrication of polycaprolactone-calcium phosphate scaffolds for tissue engineering, Biomaterials 27 (2006) 4399–4408.

[44] R.A. MacDonald, C.M. Voge, M. Kariolis, J.P. Stegemann, Carbon nanotubes increase the electrical conductivity of fibroblast-seeded collagen hydrogels, Acta Biomater. 4 (2008) 1583–1592.

[45] S.F. Nagueh, G. Shah, Y. Wu, G. Torre-Amione, N.M.P. King, S. Lahmers, C.C. Witt, K. Becker, S. Labeit, H.L. Granzier, Altered titin expression, myocardial stiffness, and left ventricular function in patients with dilated cardiomyopathy, Circulation 110 (2004) 155–162.

[46] S.M. Weis, J.L. Emery, K.D. Becker, D.J. McBride, J.H. Omens, A.D. McCulloch, Myocardial mechanics and collagen structure in the osteogenesis imperfecta murine (Oim), Circ. Res. 87 (2000) 663–669.

[47] C. Coirault, J.L. Samuel, D. Chemla, J.C. Pourny, F. Lambert, F. Marotte, Y. Lecarpentier, Increased compliance in diaphragm muscle of the cardiomyopathic Syrian hamster, J. Appl. Physiol. 85 (1998) 1762–1769.

[48] J.H. Omens, Stress and strain as regulators of myocardial growth, Prog. Biophys. Mol. Biology 69 (1998) 559–572.

[49] S.R. Shin, H. Bae, J.M. Cha, J.Y. Mun, Y.-C. Chen, H. Tekin, H. Shin, S. Farshchi, M. R. Dokmeci, S. Tang, A. Khademhosseini, Carbon nanotube reinforced hybrid microgels as scaffold materials for cell encapsulation, ACS Nano 6 (2012) 362–372.
[50] A.M. Beese, S. Sarkar, A. Nair, M. Naraghi, Z. An, A. Moravsky, R.O. Loutfy, M.J. Buehler, S.T. Nguyen, H.D. Espinosa, Bio-inspired carbon nanotube-polymer composite yarns with hydrogen bond-mediated lateral interactions, ACS Nano 7 (2013) 3434–3446.
[51] K.W. Putz, C.A. Mitchell, R. Krishnamoorti, P.F. Green, Elastic modulus of single-walled carbon nanotube/poly(methyl methacrylate) nanocomposites, J. Polym. Sci. B Polym. Phys. 42 (2004) 2286–2293.
[52] S. Ahadian, J. Ramón-Azcón, M. Estili, X. Liang, S. Ostrovidov, H. Shiku, M. Ramalingam, K. Nakajima, Y. Sakka, H. Bae, T. Matsue, A. Khademhosseini, Hybrid hydrogels containing vertically aligned carbon nanotubes with anisotropic electrical conductivity for muscle myofiber fabrication, Sci. Rep. 4 (2014) 4271.
[53] N. Saito, H. Haniu, Y. Usui, K. Aoki, K. Hara, S. Takanashi, M. Shimizu, N. Narita, M. Okamoto, S. Kobayashi, H. Nomura, H. Kato, N. Nishimura, S. Taruta, M. Endo, Safe clinical use of carbon nanotubes as innovative biomaterials, Chem. Rev. 114 (2014) 6040–6079.
[54] Z. Gao, J.A. Varela, L. Groc, B. Lounis, L. Cognet, Toward the suppression of cellular toxicity from single-walled carbon nanotubes, Biomater. Sci. 4 (2016) 230–244.
[55] J. Ramón-Azcón, S. Ahadian, R. Obregón, H. Shiku, M. Ramalingam, T. Matsue, Applications of carbon nanotubes in stem cell research, J. Biomed. Nanotechnol. 10 (2014) 2539–2561.
[56] S. Ahadian, R. Obregón, J. Ramón-Azcón, G. Salazar, H. Shiku, M. Ramalingam, T. Matsue, Carbon nanotubes and graphene-based nanomaterials for stem cell differentiation and tissue regeneration, J. Nanosci. Nanotechnol. 16 (2016) 8862–8880.
[57] S.S. Nunes, J.W. Miklas, J. Liu, R. Aschar-Sobbi, Y. Xiao, B. Zhang, J. Jiang, S. Massé, M. Gagliardi, A. Hsieh, N. Thavandiran, M.A. Laflamme, K. Nanthakumar, G.J. Gross, P.H. Backx, G. Keller, M. Radisic, Biowire: a platform for maturation of human pluripotent stem cell-derived cardiomyocytes, Nat. Methods 10 (2013) 781–787.